Sensors & Transducers, Vol. 203, Issue 8, August 2016, pp. 16-23

Sensors & Transducers

http://www.sensorsportal.com

Heat Transfer Correlations for Free Convection from Suspended Microheaters

[1, 2, 3, 4, 5, *] David GOSSELIN, [3, 4, 5] Didier CHAUSSY, [3, 4, 5] Naceur BELGACEM, [1, 2] Fabrice NAVARRO and [1, 2] Jean BERTHIER

[1] Univ. Grenoble Alpes F-38000 Grenoble, France
[2] CEA, LETI, MINATEC Campus, F-38054, Grenoble, France
[3] University Grenoble Alpes, LGP2, F-38000 Grenoble, France
[4] CNRS, LGP2, F-38000 Grenoble, France
[5] Agefpi, LGP2, F-38000 Grenoble, France
[*] E-mail: david.gosselin@cea.fr

Received: 29 July 2016 /Accepted: 28 August 2016 /Published: 31 August 2016

Abstract: Portability and autonomy for biomedical diagnostic devices are two rising requirements. It is recognized that low-energy heating of such portable devices is of utmost importance for molecular recognition. This work focuses on screen-printed microheaters based on on Joule effect, which constitute an interesting solution for low-energy heating.

An experimental study of the natural convection phenomena occurring with such microheaters is conducted. When they are suspended in the air, and because of the thinness of the supporting film, it is shown that the contributions of both the upward and downward faces have to be taken into account. A total Nusselt number and a total convective heat transfer coefficient have been used to describe the natural convection around these microheaters. In addition a relation between the Nusselt number and the Rayleigh number is derived, leading to an accurate prediction of the heating temperature (MRE < 2 %). *Copyright © 2016 IFSA Publishing, S. L.*

Keywords: Micro-heater, Natural convection, Low Rayleigh, Screen-printing, Joule effect.

1. Introduction

Microfluidic is a very promising technology to improve biomedical devices and to provide diagnostic tools for the developing world [1-2]. The World Health Organization (WHO) has introduced a list of requirements that an ideal diagnostic tool intended for the developing world must meet [3]. It can be abbreviated with the acronym ASSURED: Affordable, Sensitive, Specific, User-friendly, Rapid and Robust, Equipment-free and Delivered. In order to comply with these criteria diagnostic tools should be autonomous, low-cost and portable. In other words all the required functions must be integrated within the diagnostic device. To avoid the need of bulky and costly equipment, the motion of fluid is usually generated by capillary forces [4-5] and detection by naked eyes or with smartphone camera is preferred [6-7]. Amongst all the necessary functions for such type of devices, heating is one of the most important. For example, it is required for DNA amplification. It is also recognized that biological processes work better at a temperature of 37 °C.

A widely used approach is to take advantage of Joule effect to heat up locally the device [8-9]. Although it needs a power supply, this method remains

acceptable for portable devices as soon as it has a low power consumption and can rely on portable pocket batteries.

A common issue for Joule microheaters is their miniaturization in order to integrate them in microfluidic devices. Numerous studies have been published in the case of heating plates of dimensions comprised between few centimeters and meters [10-12]. However the case of microheaters is much less reported in the literature. In fact for such small heaters the characteristic length, defined as the area/perimeter ratio, highly depends on the dimensions. A small change of the dimensions can then greatly affect the heating temperature of the microheater.

In this work, the natural convection occurring above and below screen-printed microheaters is investigated. First the contributions of the upward and downward faces of the microheater are analyzed. A total Nusselt number and a total convective heat transfer coefficient are used to better describe these two phenomena. Then, it is demonstrated that the total Nusselt number (Nu) of such microheaters evolves accordingly to the 1/8-power of the Rayleigh number (Ra). Knowing this relation, the total convective heat transfer coefficient can be calculated and the prediction of the heating temperature as a function of the applied voltage can be achieved with a mean relative error (MRE) less than 2 %.

2. Materials and Methods

2.1. The Micro-heaters

The microheaters have been made by the screen-printing of a resistive carbon ink on a 125 µm-thick PET (Polyethylene terephthalate) film. Silver ink was used for the connections. All the screen-printings were done by Séribase industrie (Château-Gontier, France). The thickness of these screen-printed layers is about 10 µm. A typical heating elements is depicted in Fig. 1.

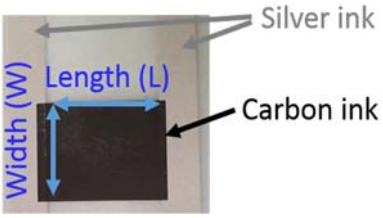

Fig. 1. Example of a screen-printed microheater used for this study.

Microheaters with varying dimensions have been designed. The width W of these devices is ranging from 11 mm to 20 mm and their length L between 5 mm and 20 mm. Such microheaters are able to provide a fast – the equilibrium temperature is reached in less than 30 s – and stable heating over one hour (Fig. 2).

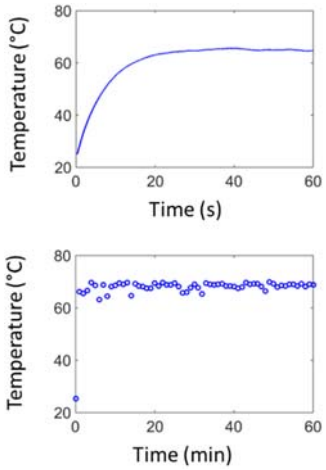

Fig. 2. The microheaters used can provide a fast (top) and stable heating (bottom).

Five elements have been used in this study to establish a relation between the Nusselt number and the Rayleigh number. These five elements have been chosen to encompass a wide range of microheater shapes, i.e. a large range of characteristic length L_c (see Table 1) which is defined as the ratio between the area of the plate A and its perimeter p:

$$L_c = \frac{A}{p} = \frac{W * L}{2 * (W + L)} \quad (1)$$

Table 1. Geometrical data of the microheaters #1 to #5 used for the study.

Element #	1	2	3	4	5
Length (mm)	5	5	12	20	20
Width (mm)	11	17	15	12	20
Lc (mm)	1.72	1.93	3.33	3.75	5

Other heating devices are used afterwards to check the validity of the law derived in this work. The dimensions of these elements are summurized in Table 2.

Table 2. Geometrical data of the heating devices used to comfirm the derived equations.

Element #	6	7	8	9	10
Length (mm)	5	10	15	16	15
Width (mm)	20	17	12	17.5	20
Lc (mm)	2	3.15	3.33	4.18	4.29

2.2. The Experimental Set-up

During the experiments, the heating device was maintained suspended in the air by crocodile clips connected to the voltage supply. The thermal measurments were perfomed with a ThermoVision A20 thermal camera (FLIR Systems, USA) controlled

with the ThermaCAM Researcher Pro software. Fig. 3 shows the experimental set-up.

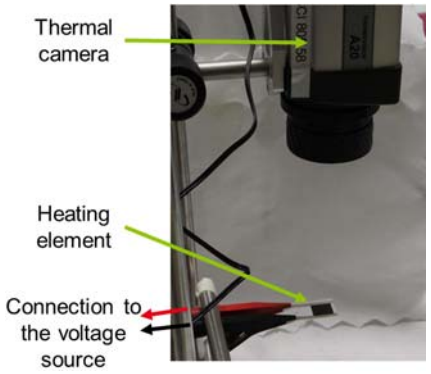

Fig. 3. Experimental set-up for temperature measurements.

Prior to making quantitative temperature measurements, the emissivity factor of the carbon ink has been determined. The ThermaCAM Researcher Pro software offers the possibility to calculate this factor. This is done by heating up a device at a given temperature and indicating the expected temperature to the software. At 60°C, the emissivity of the carbon ink used in this study was measured to be 0.73.

The quantitative temperature measurements were then obtained by exporting the pictures of the thermal camera in black and white with a linear scale. These images are then processed with ImageJ to determine the average gray level of the heating area. Doing a cross multiplication with the linear scale allows to obtain the average temperature of the heating element. Note that, in the rest of this paper the temperature of an element T always refers to this average temperature.

2.3. Resistivity Measurements

In order to provide adequate results, the evolution of the resistance of these heaters according to the temperature had to be determined. This was done by first heating the elements up to around 80°C by Joule effect and then unplugging the voltage supply. While the devices were cooling down, measurements of both the temperature and the resistance were performed. The resistance of the elements were measured and displayed with an ohmmeter. In the particular case of these experiments, the temperature measurements were directly done and displayed with the FLIR software. This allows a live recording of the temperature and the associated resistance by filming the two displays at the same time.

3. Results and Discussions

The following sections focus on the natural convection of these microheaters. On the one hand, in Section 3.2, an global approach based on equations found in the litterature is compared to the experimental data. On the other hand, in Section 3.3, the experimental data are directly used to derive an expression between the Rayleigh and the Nusselt numbers. In addition, it will be shown that the heating temperature can be accurately predicted as a function of the applied voltage.

Both of these approaches are based on a relation beween two dimensionless numbers: the Nusselt number and the Rayleigh number. The Rayleigh number expression is

$$Ra = Gr * \mathrm{Pr} = \frac{g * \beta * (T - T_\infty) * Lc^3 * \mathrm{Pr}}{\nu^2}, \quad (2)$$

where *Gr* is the Grashof number, *Pr* is the Prandtl number (for the fluid, here the air), *g* is the gravity acceleration, T_∞ is the room temperature and β (resp. υ) is the thermal expansion coefficient (resp. the viscosity) of the fluid (here the air).

The Nusselt number is defined as

$$Nu = \frac{h * Lc}{k}, \quad (3)$$

where *h* is the convective heat tranfer coefficient and *k* the thermal conductivity of the fluid (here the air).

While the Rayleigh number can be calculated from the experimental temperature measurements (and from handbook values for the physical properties of the air), an unknown remains for the Nusselt number: the convective heat transfer coefficient h. It can be determined by balancing the heat flux equations over the system for the steady state regime.

Based on the schematic of Fig. 4, this balance can be written:

$$\varphi_g - \varphi_U^{conv} = \varphi_{PET}^{cond} = \varphi_D^{conv} \quad (4)$$

with $\varphi_g = U^2/R(T)$

$$\varphi_U^{conv} = h_U * A * (T_U - T_\infty),$$

$$\varphi_{PET}^{cond} = k_{PET} * A/e * (T_U - T_D),$$

$$\varphi_D^{conv} = h_D * A * (T_D - T_\infty),$$

where U is the applied voltage, R(T) is the resistance of the microheater which depends on its temperature, k_{PET} is the thermal conduction of the PET, e is the thickness of the PET sheet, h_U (resp. h_D) is the convective heat transfer coefficient of the upward (resp. downward) face and T_U (resp. T_D) is the temperature of the upward (resp. downward) face.

By using only the right and left terms of Eq. (4) it can be writen that:

$$\frac{U^2}{R(T)} = h_U * A * (T_U - T_\infty) + h_D * A * (T_D - T_\infty) \quad (5)$$

Assuming that $T_U \approx T_D$ (it will be discussed later), and defining the total convective heat transfer coefficient *h* as

$$h = h_U + h_D \quad (6)$$

the Eq. (5) can be writen

$$\frac{U^2}{R(T)} = h * A * (T - T_\infty) \quad (7)$$

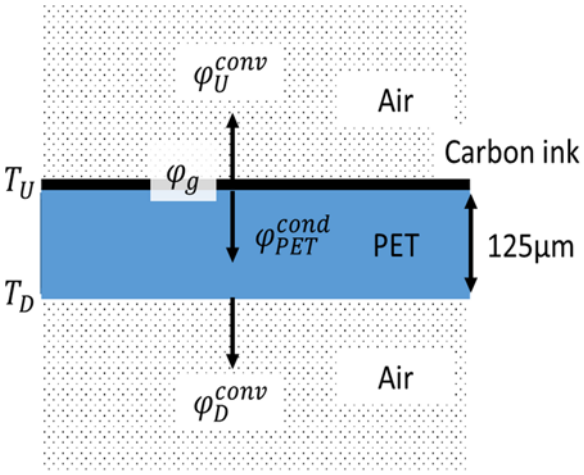

Fig. 4. Schematic of the heat fluxes within the system.

And finally the expression of the Nusselt number can be cast under the following form:

$$Nu = \frac{U^2 * Lc}{R(T) * A * (T - T_\infty) * k}, \quad (8)$$

where the only unknown remaining is the evolution of the resistance of the microheaters accordingly to the temperature which will be determined in the next section.

Let us now discuss the assumption $T_U \approx T_D$. This assumption seems reasonnable because the thickness of the PET sheet is very small: 125 µm. In fact, the temperature difference between the two faces can be estimated from Eq. (4) by considering that half of the generated heat flux goes through the PET sheet:

$$(T_U - T_D) = \frac{e}{k_{PET} * A} * \frac{1}{2} * U^2 / R(T) \quad (9)$$

Doing some numerical applications we found that the temperature difference is of the order of (or less than) 1 °C (Fig. 5 (a)) which gives an error of the order of 1 % (Fig. 5 (b)) if one assumes that these two temperatures are equals. Thus as a first order approximation, one can consider that $T_U \approx T_D$. Note that equalizing T_U and T_D does not mean that the heat flux through the PET given by (4) is negligible, because this flux is proportional to $(T_U - T_D)/e$.

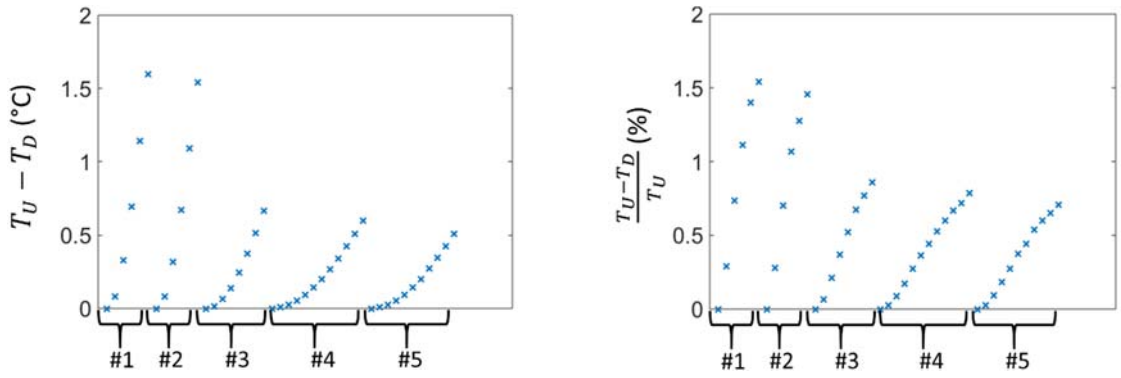

(a) (b)

Fig. 5. (a) Temperature difference between the upward face and the downward face of the microheaters calculated according to Eq. (9). (b) Error in percent for considering that both of the faces are at the same temperature.

3.1. Temperature Dependency of the Resistivity

The dependency of the resistivity of the carbon ink is an essential data to calculate the accurate input power. Indeed for a given voltage *U* the power *P* is given by:

$$P = \frac{U^2}{R(T)}, \quad (10)$$

where *R(T)* is the resistance which writes.

$$R(T) = \rho(T) * \frac{L}{W * e} = R_{\blacksquare}(T) * \frac{L}{W}, \quad (11)$$

where ρ is the bulk resistivity and $R_{\blacksquare}$ is the sheet resistance.

The $R_{\blacksquare}$ coefficient is often used to characterize the resistance of thin films. It is a normalization of the resistance by the width and the length of the element. The values of the sheet resistance according to the temperature for the microheaters listed Table 1 are presented in Fig. 6.

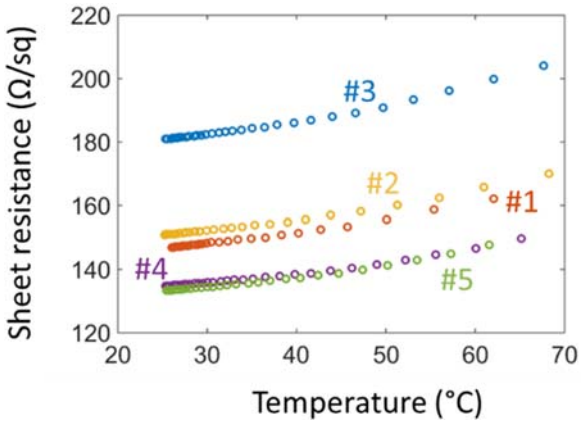

Fig. 6. Evolution of the sheet resistance $R_{\blacksquare}$ against the temperature for microheaters #1 to #5.

This figure shows that the dependency on temperature of the sheet resistance is very similar for the five elements. However there is a constant shift between different elements. This shift is due to the difference in thickness of these elements. Indeed, even if all these microheaters were screen-printed on the same PET sheet, the thickness of the carbon layer is not homogenous all over the PET sheet. To go one stage further, a normalized bulk resistivity is defined:

$$\frac{\rho(T)}{\rho(27.6°C)} = \frac{R_{\blacksquare}(T)}{R_{\blacksquare}(27.6°C)} \quad (12)$$

Fig. 7 shows a plot of this normalized bulk resistivity as a function of the temperature for the microheaters #1 to #5. The data points of all five elements are well fitted with a second order polynomial equation ($R^2 > 0.99$).

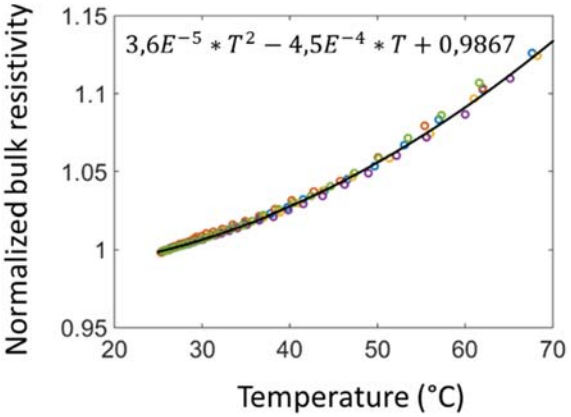

Fig. 7. Evolution of the normalized bulk resistivity $\frac{\rho(T)}{\rho(27.6°C)}$ according to the temperature for microheaters #1 to #5.

The resistance of a microheater at a given temperature can then be calculated according to:

$$R(T) = R(27.6°C) * (3.6E^{-5} * T^2 - 4.5E^{-4} * T + 0.9867) \quad (13)$$

In addition, the difference of the resistance between 27.6 °C and the ambient temperature is very small. In fact considering that the ambient temperature is 21 °C, the difference is only 0.7 %. Thus the resistance at a given temperature can be calculated using the resistance of the same microheater measured at the ambient temperature according to:

$$R(T) \approx R(T_{amb}) * (3.6E^{-5} * T^2 - 4.5E^{-4} * T + 0.9867) \quad (14)$$

Now that the evolution of the resistance with the temperature has been derived, the experimental Nusselt number can be calculated from Eq. (8).

3.2. A Global Approach

In this section, the experimental Rayleigh and Nusselt numbers will be compared to a published theoretical relation between these two numbers [10]. In this theoretical approach the expression of the Nusselt number is first expressed in a thin-layer approximation (Nu^T) and is afterwards corrected into the fully laminar Nusselt number (Nu). In the present study, because of the low Rayleigh numbers ($<10^3$), the convective flow around the microheaters can be considered as laminar. Thus the turbulent Nusselt number can be neglected. In other words, the laminar Nusselt number is equivalent to the Nusselt number.

With this method, the expression between the Nusselt and the Rayleigh numbers depends only on the geometry (flat plates, cylinder, etc.) and on the orientation (vertical, horizontal, etc.); whereas with the local approach discussed in the next section this relation will also depend on the order of magnitude of the Rayleigh number.

Because the heating devices are suspended in air during the experiments, natural convection occurs at the upward and downward faces of the devices. To model this double phenomena a total Nusselt number was used:

$$Nu = Nu_U + Nu_D \quad (15)$$

Note that the definition of such a total Nusselt number is consistent with the definition of the total heat transfer coefficient of Eq. (6). In fact

$$Nu = Nu_U + Nu_D = \frac{h_U * L_c}{k} + \frac{h_D * L_c}{k} = \frac{h * L}{k} \quad (16)$$

The relations between the Rayleigh and the Nusselt numbers are extracted from ref [10]. On the one hand, for an upward-facing plate (index U), the equation writes:

$$Nu_U^T = 0.835 \frac{0.671}{\left(1 + \left(0.492/Pr\right)^{9/16}\right)^{4/9}} Ra^{1/} \quad (17)$$

And the laminar Nusselt number is given by

$$Nu_U = \frac{1.4}{ln\left(1 + {}^{1.4}/_{Nu_U^T}\right)} \quad (18)$$

On the other hand, for a downward-facing plate (index D):

$$Nu_D^T = \frac{0.527}{\left(1 + \left({}^{1.9}/_{Pr}\right)^{0.9}\right)^{2/9}} Ra^{1/5} \quad (19)$$

and

$$Nu_D = \frac{2.5}{ln\left(1 + {}^{2.5}/_{Nu_D^T}\right)} \quad (20)$$

Fig. 8 confirms that the introduction of this total Nusselt number is necessary to describe the experiments. In fact the downward-facing contribution (blue triangles) is of the same order of magnitude than the upward-facing contribution (magenta triangles) and thus these two aspects have to be taken into account. The total Nusselt number (red solid line) of Eq. (15), allows a better description than each of the two Eq. (18) and Eq. (20) taken separately. However the data points still lie within about 15 ± 4 % above Eq. (15).

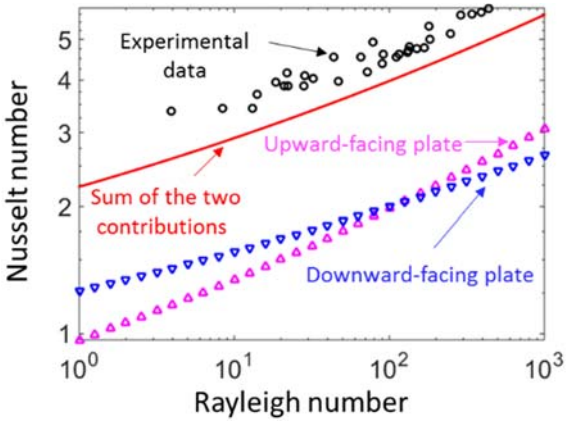

Fig. 8. Comparison between experimental data (black circles) and different equations: the upward-facing Eq. (18) (magenta triangles), the downward-facing Eq. (20) (blue triangles) and Eq. (15) (red line).

In addition to this error, the complexity of the equations used makes this approach not suitable to calculate the total convective heat transfer coefficient and predict the heating temperature of these devices. That is why in the next section focus will be put on a local approximation of the relation between the Nusselt and the Rayleigh numbers. As we shall see, this will allow the calculation of the total convective heat transfer coefficient and an accurate prediction of the heating temperatures.

3.3. A Local Approach: Total Convective Heat Transfer Coefficient Calculation and Prediction of the Heating Temperature

In a simpler manner than in the previous section, natural convection phenomena are often modeled by expressing the Nusselt number as a power-function of the Rayleigh number:

$$Nu = a\, Ra^n, \quad (21)$$

where a and n are constants which depend on the order of magnitude of the Rayleigh number [11-12].

Fig. 9 shows the fitting of the experimental data points (of the five microheaters listed in Table 1) with Eq. (21). This fitting is done with the polyfit function of the MATLAB software. It is found that these experimental data points can be well fitted with a 1/8-power function:

$$Nu = 2.65 * Ra^{0.124} \sim 2.65\, Ra^{1/8} \quad (22)$$

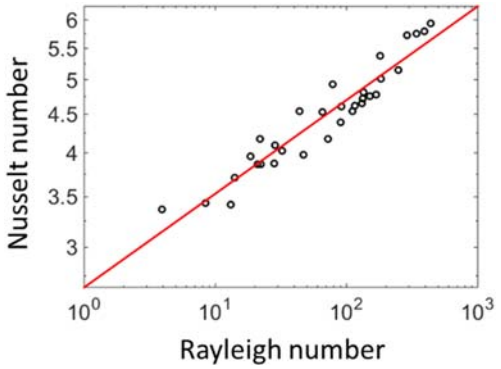

Fig. 9. Black circles: Experimental data. Red solid line: Fit of these experimental data with Eq. (22).

Subtituting Eq. (2) and Eq. (3) in Eq. (22) leads to the determination of an expression for the total convective heat transfer coefficient:

$$h = 2.65 * k * \left(\frac{g * \beta * (T - T_\infty) * Pr}{\nu^2}\right)^{\frac{1}{8}} * L_c^{-5/} \quad (23)$$

Fig. 10 depicts the evolution of the total convective heat transfer coefficient according to the temperature of the element and to its characteristic length (L_c). It shows that this coefficient highly depends on the characteristic length as it can be expected for heaters of such small dimensions. It also depends on the temperature of the microheater but in a lesser degree as soon as the temperature exceeds 40 °C. Values of this coefficient for the ten microheaters used in this study at either 40 °C or 90 °C can be found in Table 3. In particular, it can be noticed that the total convective heat transfer coefficient of the element #1 is twice as high as the one of the element #5.

Table 3. Numerical application of the total convective heat transfer coefficient (at 40 °C and 90 °C) for the different microheaters used in this study. Note that in this table the elements have been ordered by increasing Lc and not by element number.

Element #	**1**	**2**	**6**	**7**	**8**	**3**	**4**	**9**	**10**	**5**
Lc (mm)	1.72	1.93	2	3.15	3.33	3.33	3.75	4.18	4.29	5
h at 40°C (W/m²/K)	53.3	49.6	48.5	36.5	35.3	35.3	32.7	30.6	30.1	27.4
h at 90°C (W/m²/K)	63.9	59.4	58.1	43.8	42.3	42.3	39.2	36.7	36.1	32.8

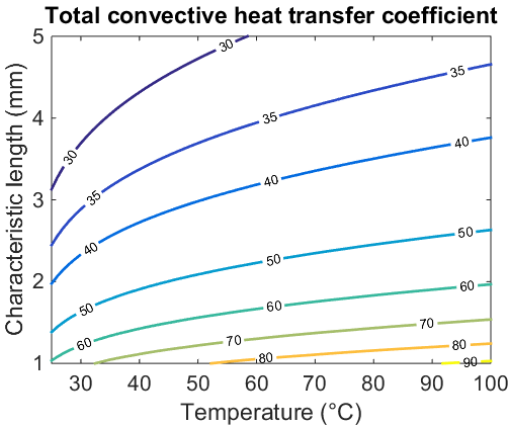

Fig. 10. Evolution of the total convective heat transfer coefficient according to the temperature of the element and to its characteristic length.

Finally combining Eq. (23) and Eq. (7) allows the authors to express the voltage needed to obtain a desired temperature:

$$U = \sqrt{2.65 * R(T) * A * k * \left(\frac{g * \beta * Pr}{\nu^2}\right)^{\frac{1}{8}} * L_c^{-\frac{5}{8}} * (T - T_\infty)^{\frac{9}{8}}} \quad (24)$$

Fig. 11 presents the experimental data points of seven microheaters (the five listed in Table 2 and two of Table 1) along with the prediction made using Eq. (24).

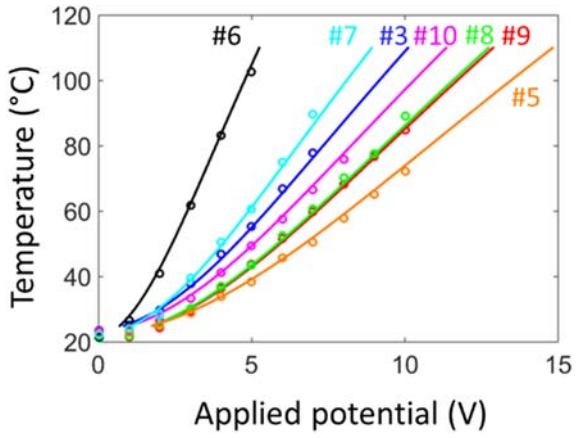

Fig. 11. Comparison between prediction (solid lines) and experimental data (circles) for different heaters (labelled accordingly to Table 1 and Table 2).

The experimental data points of the three last microheaters of Table 1 have not been plotted for more clarity. This figure shows that the derived expression allows an accurate prediction of the heating temperature of the microheaters (MRE<2 %). In particular, the accurate prediction of the heating temperatures for the five microheaters listed in Table 2 – which have not been used to obtain the equations – demonstrates the validity of the different derived equations.

4. Conclusions

In this work a study on the natural convection ocurring above and below screen-printed microheaters has been performed. These microheaters relies on Joule effect and are of utmost interest for an integration on microfluidic portable diagnostic tools. In fact the heating temperature is reached within 30 s and is then stable over one hour allowing to perform biological analyses.

It has been shown that when suspended in the air, because of the thinness of the supporting film, the contributions of both the upward and downward faces have to be taken into account. To do so, a total convective heat transfer coefficient and a total Nusselt number have been used. It has also been demonstrated that for such microheaters the total Nusselt number evolves accordingly to the 1/8-power of the Rayleigh number. Finally on the basis of this relation, calculations of the total convective heat transfer coefficient can be done and the prediction of the heating temperatures can be accurately performed.

References

[1]. E. K. Sackmann, A. L. Fulton, D. J. Beebe, The present and future role of microfluidics in biomedical research, *Nature*, Vol. 507, No. 7491, 2014, pp. 181-189.

[2]. G. M. Whitesides, Cool, or simple and cheap? Why not both?, *Lab Chip*, Vol. 13, 2013, pp. 11-13.

[3]. H Kettler, K White, S Hawkes, Mapping the landscape of diagnostics for sexually transmitted infections, *WHO/TDR*, Geneva, 2004.

[4]. Gervais L., Capillary microfluidic chips for point-of-care testing: from research tools to decentralized medical diagnostics, PhD Thesis, *Ecole Polytechnique de Lausanne*, 2011.

[5]. Berthier J., Brakke K. A., Furlani E. P., Karampelas I. H., Poher V., Gosselin D., Cubizolles M., Pouteau P.,

Whole blood spontaneous capillary flow in narrow V-groove microchannels, *Sensors and Actuators B: Chemical*, Vol. 206, 2015, pp. 258-267.

[6]. Martinez A. W., Phillips S. T., Butte M. J., Whitesides G. M., Patterned Paper as a Platform for Inexpensive, Low-Volume, Portable Bioassays, *Angewandte Chemie International Edition*, Vol. 46, No. 8, 2007, pp. 1318-1320.

[7]. Koesdjojo M. T., *et al*., Cost Effective Paper-Based Colorimetric Microfluidic Devices and Mobile Phone Camera Readers for the Classroom, *Journal of Chemical Education*, Vol. 92, No. 4, 2015, pp. 737-741.

[8]. Moschou D., *et al*., All-plastic, low-power, disposable, continuous-flow PCR chip with integrated microheaters for rapid DNA amplification, *Sensors and Actuators B: Chemical*, Vol. 199, 2014, pp. 470-478.

[9]. Noguchi Y., Kawai A., Local Heating System Integrated with Platinum Micro Heater and Photopolymer Microfluidic Channel, *Journal of Photopolymer Science and Technology*, Vol. 26, 2013, pp. 713-716.

[10]. G. D. Raithby, K. G. T. Hollands, Natural convection, in W. M. Rohsenow, J. P. Hartnett, Y. I. Cho, Handbook of Heat Transfer, 3rd edition, *McGraw-Hill Education,* 1998.

[11]. Massimo Corcione, Heat Transfer Correlation for Free Convection from Upward-Facing Horizontal Rectangular Surfaces, *WSEAS Transactions on Heat and Mass Transfer*, Vol. 2, No. 3, 2007, pp. 48-60.

[12]. I. Martorell, J. Herrero, F. X. Grau, Natural convection from narrow horizontal plates at moderate Rayleigh numbers, *Int. J. Heat Mass Transfer*, Vol. 46, No. 13, 2003, pp. 2389-2402.
